NANO LETTERS

Letter

pubs.acs.org/NanoLett

The Strong Influence of Internal Stresses on the Nucleation of a Nanosized, Deeply Undercooled Melt at a Solid−Solid Phase Interface

Kasra Momeni,[†] Valery I. Levitas,*[,†,‡,§,∥] and James A. Warren[∥]

[†]Department of Aerospace Engineering, [‡]Department of Mechanical Engineering, [§]Material Science and Engineering, Iowa State University, Ames, Iowa 50011, United States

[∥]Materials Science and Engineering Division, Material Measurement Laboratory, National Institute of Standards and Technology, Gaithersburg, Maryland 20899, United States

Supporting Information

ABSTRACT: The effect of elastic energy on nucleation and disappearance of a nanometer size intermediate melt (IM) region at a solid−solid (S_1S_2) phase interface at temperatures 120 K below the melting temperature is studied using a phase-field approach. Results are obtained for broad range of the ratios of S_1S_2 to solid−melt interface energies, k_E, and widths, k_δ. It is found that internal stresses only slightly promote barrierless IM nucleation but qualitatively alter the system behavior, allowing for the appearance of the IM when $k_E < 2$ (thermodynamically impossible without mechanics) and elimination of what we termed the IM-free gap. Remarkably, when mechanics is included within this framework, there is a drastic (16 times for HMX energetic crystals) reduction in the activation energy of IM critical nucleus. After this inclusion, a kinetic nucleation criterion is met, and thermally activated melting occurs under conditions consistent with experiments for HMX, elucidating what had been to date mysterious behavior. Similar effects are expected to occur for other material systems where S_1S_2 phase transformations via IM take place, including electronic, geological, pharmaceutical, ferroelectric, colloidal, and superhard materials.

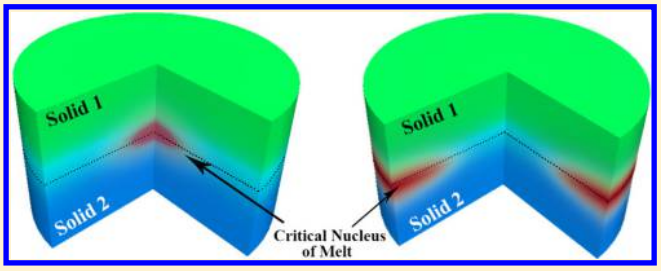

KEYWORDS: *Intermediate melt, phase field approach, solid−melt−solid interface, nucleation, internal stresses*

In this study, we investigate the appearance of phases at a solid−solid (S_1S_2) boundary, detailing the influence of processes within few nanometer thick phase interface, including its structure and stress state. It is found that the S_1S_2 interface tends to reduce its energy via elastic stress relaxation and restructuring. Specifically, restructuring can occur via the nucleation of a nanometer-scale intermediate melt (IM) at the S_1S_2 boundary at temperatures well below the bulk melting temperature. This mechanism was proposed for $\beta \leftrightarrow \delta$ phase transformations (PTs) in energetic organic HMX crystals[1,2] at undercoolings of 120 K in order to explain puzzling experimental data in refs 3 and 4. The appearance of the IM at these temperatures allowed for a relaxation of elastic energy at the S_1S_2 phase interface, making the transition energetically favorable. This mechanism explained, both quantitatively and qualitatively, 16 nontrivial experimental phenomena.[2] In addition to stress relaxation and elimination of interface coherency, the IM eliminates athermal friction and alters the interface mobility. Along related lines, the mechanism of crystal−crystal and crystal−amorphous PTs via intermediate (or virtual) melting for materials (like water) where increasing the pressure leads to a reduction in the melting temperature was suggested in ref 5. Amorphization via virtual melting was claimed in experiments for Avandia (Rosiglitazone), an antidiabetic pharmaceutical, in ref 6. Also, solid−solid PT via IM and surface-induced IM in $PbTiO_3$ nanofibers was observed experimentally and treated thermodynamically in ref 7. In this case, melting within the S_1S_2 interface was caused by reduction in the total interface energy and relaxation of internal elastic stresses. And in subsequent investigations, it was found that relaxation of external deviatoric stresses under very high strain rate conditions could cause melting at undercoolings of 4000 K.[8] The important role of these phenomena in the relaxation of stress in crystalline systems is given in ref 9. Most recently, the transition between square and triangular lattices of colloidal films of microspheres via an IM was directly observed in ref 10. However, there are some essential inconsistencies in the thermodynamic and kinetic interpretation of this phenomenon in ref 10. While it is stated that crystal−crystal transformation occurs below the bulk melting temperature T_m, the bulk driving force for melting is considered to be positive, which is possible above T_m only. In contrast to the statement in ref 10, crystal−

Received: November 14, 2014
Revised: February 21, 2015
Published: March 19, 2015

DOI: 10.1021/nl504380c
Nano Lett. 2015, 15, 2298−2303

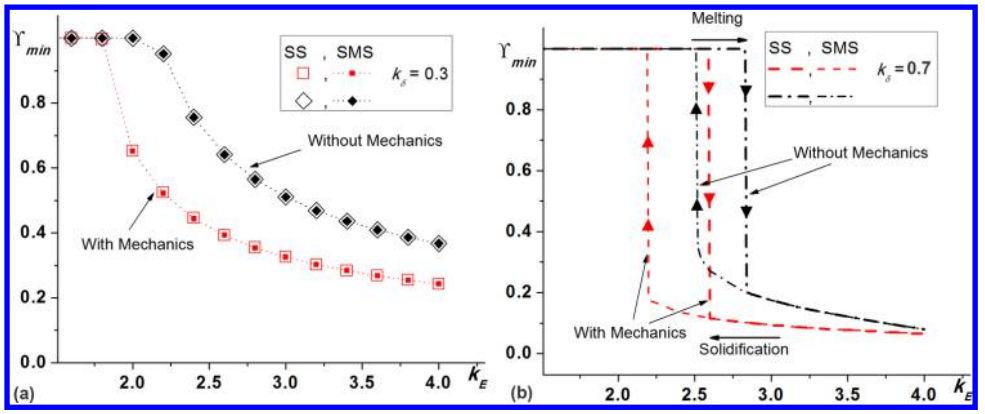

Figure 1. Effect of internal elastic stresses on thermodynamically equilibrium solutions as a function of k_E. Initial conditions are shown in boxes and correspond to S_1S_2 (designated as SS) and S_1MS_2 (designated as SMS) interfaces. Value of Υ_{min} is shown for problems without and with mechanics at $\theta = \theta_e = 432$ K, which is 120 K below the melting temperature. (a) Continuous premelting/resolidification for small $k_\delta = 0.3$, and (b) jumplike IM and resolidification for $k_\delta = 0.7$. Allowing for elastic energy that relaxes during intermediate melting promotes melting for all cases.

crystal transformation via intermediate (virtual) melting have been discussed for a decade, indeed significantly below melting temperature[1,2,5−9,11,12] and with much more general thermodynamic and kinetic description.

In the above treatments of this phenomena, the theoretical approach was limited to simplified continuum thermodynamics. Recently, however, we introduced a phase-field approach for the S_1S_2 phase transformation via IM and the formation of disordered interfacial phases both without[11] and with[12] mechanical effects. This approach yielded a more detailed picture of the interface, including the appearance of a "partial" IM and the substantial influence of the parameter k_δ, an effect necessarily not present in sharp-interface theories. In refs 11 and 12, the effect of relaxation of internal stresses was briefly investigated for the case of barrierless IM nucleation, and nucleation via a critical nucleus (CN) was not explored. In fact, results in ref 11 for CN appeared to eliminate it as a mechanism for stress relaxation, as the CN had too high an activation energy to explain observation of macroscopic kinetics of $\beta \leftrightarrow \delta$ PTs in HMX crystals.[1−4]

In this Letter, we employ our phase field approach to study effect of mechanics, that is, internal stresses (for different ratios k_E and k_δ) on the thermodynamics, kinetics, and structure of IM within a S_1S_2 interface, describing its appearance and disappearance due to barrierless and thermally activated processes 120 K below bulk melting temperature in a model HMX system. It is found that internal stresses only slightly promote barrierless IM nucleation but qualitatively alter the system behavior, allowing for the appearance of the IM when $k_E < 2$ (thermodynamically impossible without mechanics) and elimination of what we termed the IM-free gap. Remarkably, when mechanics is included within this framework, there is a drastic (16 times for HMX energetic crystals) reduction in the activation energy of IM critical nucleus. After this inclusion, a kinetic nucleation criterion is met, and thermally activated melting occurs under conditions consistent with experiments for HMX, elucidating what to date had been mysterious behavior.[1,2] CN at the surface of a sample is also studied.

Model. For description of PTs between three phases, a phase-field model introduced in ref 12 (and presented in Supporting Information) employs two polar order parameters: radial Υ and angular ϑ, where $\pi\vartheta/2$ is the angle between the radius vector Υ and the positive horizontal axis in the polar order parameter plane. The melt is represented by $\Upsilon = 0$ for all ϑ. Solid phases correspond to $\Upsilon = 1$; phase S_1 is described by $\vartheta = 0$ and phase S_2 is described by $\vartheta = 1$. This representation of the three phases sits in contrast to other multiphase models[13−16] that used three order parameters with a constraint that they always sum to a constant. Unlike the prior approaches, the polar variable approach has desirable property that each of the PTs: $M \leftrightarrow S_1$, corresponding to variation in Υ between 0 and 1 at $\vartheta = 0$; $M \leftrightarrow S_2$, corresponding to variation in Υ between 0 and 1 at $\vartheta = 1$; and $S_1 \leftrightarrow S_2$, corresponding to variation in ϑ between 0 and 1 at $\Upsilon = 1$, is described by single order parameter with the other fixed, which allowed us to utilize analytical solutions for each of the nonequilibrium interfaces and determine their width, energy, and velocity.[11,12] Similar to sharp-interface study of phase transformations in HMX, which is consistent with experiments,[1,2] we assume that internal stresses cannot cause nucleation of dislocations. The model was implemented in the finite element package COMSOL.[17] Material parameters have been chosen for organic HMX energetic crystal (Tables 1 and 2 in Supporting Information). Problems have been solved for different k_E and k_δ values at equilibrium temperature of two HMX solid phases, $\theta_e = 432$ K, which is 120K below the melting temperature of the δ phase, which melts and resolidifies into β phase during $\beta \rightarrow \delta$ PT. Here the values of k_E and k_δ are explored to determine their influence, partly as they are unknown; but also we expect that these parameters will be sensitive in experiments to impurities and other "alloying" effects and thus can be experimentally controlled to some degree.

For barrierless processes, a rectangular 40 nm × 300 nm with the symmetry plane at its left vertical edge, fixed lower left corner, and a stress-free boundary on the right side are considered. A vertical initial interface was placed in the middle of the sample. Two types of initial conditions have been used: (i) A stationary S_1S_2 interface, which is obtained by placing an analytical solution for a stationary stress-free interface as an initial condition (see eq 19 in Supporting Information), and (ii) a pre-existing melt confined between two solid phases (designated as S_1MS_2), which is obtained as a stationary solution with initial data corresponding to S_1MS_2 with a complete IM that is broader than in stationary solution. Parameters k_δ and k_E are explicitly defined in the Supporting Information (see eq 20 therein). Plane strain conditions in the out-of-plane direction are assumed. The domain is meshed with five elements per S_1S_2 interface width, using quadratic Lagrange

DOI: 10.1021/nl504380c
Nano Lett. 2015, 15, 2298−2303

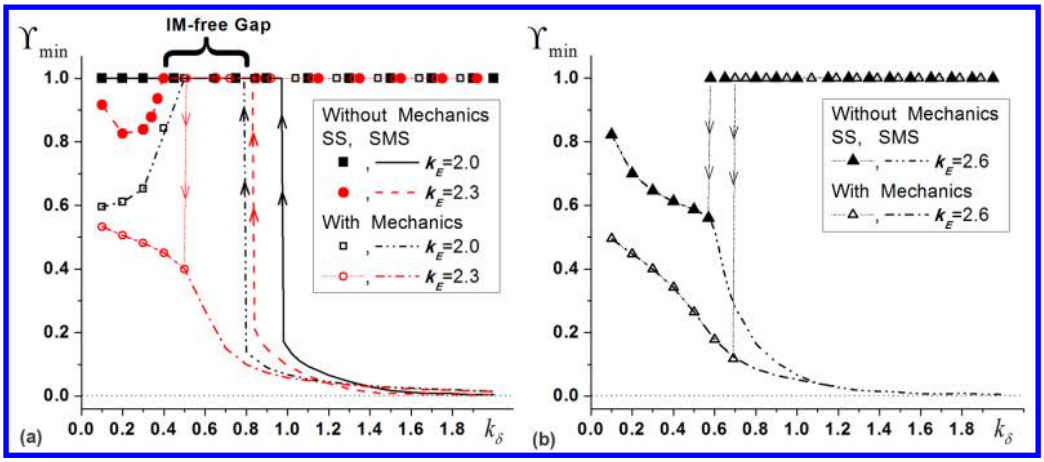

Figure 2. Mechanics and scale effects on thermodynamically equilibrium solutions Υ_{min} at $\theta = \theta_e = 432$ K for three values of k_E. Elastic energy promotes formation of melt and changes qualitatively types of behavior for some parameters.

elements. An implicit time-stepping integrator with variable-step-size backward differentiation is used with initial time step of 1 ps and a relative tolerance of 10^{-4}. The numerical model is verified by solving the time-dependent Ginzburg–Landau equations (phase fields) for the PT between two phases at different temperatures without mechanics and comparing the results with analytical solutions for the interface energy, width, velocity, and profile,[11] which indicate perfect match.

Barrierless Nucleation. Here, the effect of thermal fluctuations is neglected and barrierless PTs are studied. The IM exhibits itself as deviation of the order parameter Υ within otherwise S_1S_2 interface from 1. If the minimum value Υ_{min} reaches zero, then IM is complete; otherwise, it is incomplete IM. In Figures 1 and 2, the minimum value Υ_{min} is presented for the steady state solution using two initial conditions (states): stationary S_1S_2 and S_1MS_2 interfaces.

Results for small k_δ values in Figure 1a revealed continuous premelting/resolidification with increasing/decreasing k_E and presence of only a single solution independent of initial conditions. Allowing for internal stresses generated by misfit strain at the S_1S_2 interface promotes melt formation, that is, reduces Υ_{min}. In other words, melting results in the partial or complete relaxation in internal stresses, or stress results in an additional thermodynamic driving force for melting. Mechanics also shifts the minimum value of k_E for initiation of disordering, even below $k_E < 2.0$, which is energetically impossible without mechanics (because energy of two *SM* stress-free interfaces is larger than energy of *SS* interface). For larger $k_\delta = 0.7$ (Figure 1b) a range of k_E values is found for which two different stationary solutions exist depending on the chosen initial conditions. Solutions for Υ_{min} experience jumps from 1 to small values after reaching some critical k_E and then change continuously with increasing or decreasing k_E. Starting with IM state, decreasing k_E leads to jump to $\Upsilon_{min} = 1$. Thus, in contrast to Figure 1a, there is a clear hysteresis behavior. Internal elastic stresses reduce Υ_{min} and shift the critical k_E values for loss of stability of S_1S_2 and S_1MS_2 interfaces to lower values of k_E, as well as increase hysteresis region, thus promoting IM.

A much richer picture is observed when Υ_{min} is plotted versus scale parameter k_δ for different fixed k_E (Figure 2). Figure 2b for $k_E = 2.6$ shows that for small k_δ values, S_1S_2 interface does not exist and the only continuous reversible intermediate melting/ordering occurs with increasing/decreasing k_δ. Elastic stresses promote IM again by reducing Υ_{min}. With further increases in k_δ for the same S_1MS_2 interface, the degree of disordering increases (and reversibly decreases with decreasing k_δ), the effect of mechanics diminishes and disappears when Υ_{min} reaches zero. However, for large k_δ an alternative solution $\Upsilon_{min} = 1$ exists and if S_1S_2 interface is the initial state, it does not change. Below some critical k_δ, a jump from S_1S_2 interface to S_1MS_2 interface occurs with reducing k_δ and the elastic energy increases slightly this critical value. A reverse jump is impossible, thus S_1MS_2 interface does not transform to S_1S_2 interface barrierlessly.

For smaller $k_E = 2.0$ and 2.3, the effect of the scale parameter k_δ is nonmonotonous and thus more complex (Figure 2a). For $k_E = 2.0$ without mechanics, the only solution is the S_1S_2 interface. Elastic energy changes result qualitatively. Thus, for small k_δ the only solution contains IM; however, the degree of disordering reversibly reduces with increasing k_δ (opposite to the case with larger k_E in Figure 2b) and eventually disappears. For large k_δ, there are both (almost) complete S_1MS_2 and S_1S_2 solutions. While initial S_1S_2 does not change in this range, IM reduces degree of disordering with reducing k_δ, until IM discontinuously disappears. For intermediate k_δ, the only solution is the S_1S_2 interface. This region between two other regions where IM exists we called the IM-free gap. For $k_E = 2.3$, IM-free gap exists without mechanics but disappears with mechanics. Now, with mechanics the behavior is qualitatively similar to that for $k_E = 2.6$ (Figure 2b). Without mechanics, for small k_δ the value Υ_{min} first decreases and then increases up to $\Upsilon_{min} = 1$ (i.e., exhibits local minimum), followed by IM-free gap and then by two solutions. Thus, mechanics qualitatively changes types of barrierless behavior. However, quantitatively values Υ_{min} are not drastically affected.

Thermally Activated Nucleation. The presence of two stationary solutions in Figure 1b, corresponding to local minima of the energy, indicates existence of the third, unstable, solution equivalent to the "min–max" of energy functional corresponding to a CN between them. Critical nuclei are studied at $\theta = \theta_e = 432$ K for $k_E = 2.6$ and $k_\delta = 0.7$, that is, in the range of parameters where two solutions exist for both cases without and with mechanics (Figure 1b). Because of thermodynamic instability, CN solutions are highly sensitive to the initial conditions of the system and can be obtained by solving stationary Ginzburg–Landau and mechanics equations using an affine invariant form of the damped Newton method

DOI: 10.1021/nl504380c
Nano Lett. 2015, 15, 2298–2303

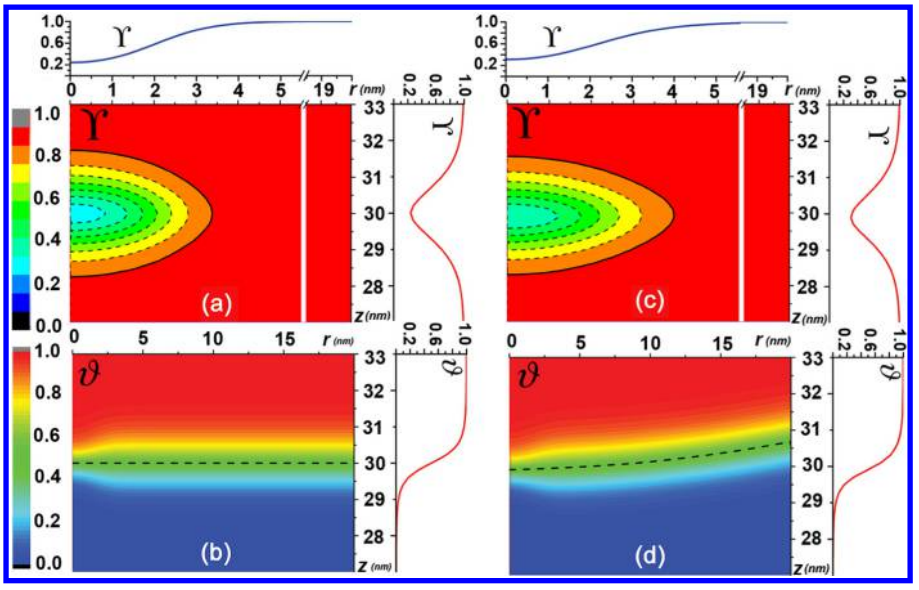

Figure 3. Structure for the CN_1 with IM at the center of a sample. Simulations are performed at θ_e = 432 K, k_δ = 0.7, and k_E = 2.6 for the cases without (a,b) and with mechanics (c,d). Profile of the order parameter $\Upsilon(r)$ along the horizontal line z = 30 nm is plotted in the top insets. Vertical insets show the profile of $\Upsilon(z)$ (top plots) and $\vartheta(z)$ (bottom plots) at r = 0. Solid line in the Υ plots corresponds to Υ = 0.9 and determines the boundary of disordered CN of IM within the S_1S_2 interface. Dotted line in the ϑ plots indicates the level line of ϑ = 0.5 and corresponds to the sharp S_1S_2 interface.

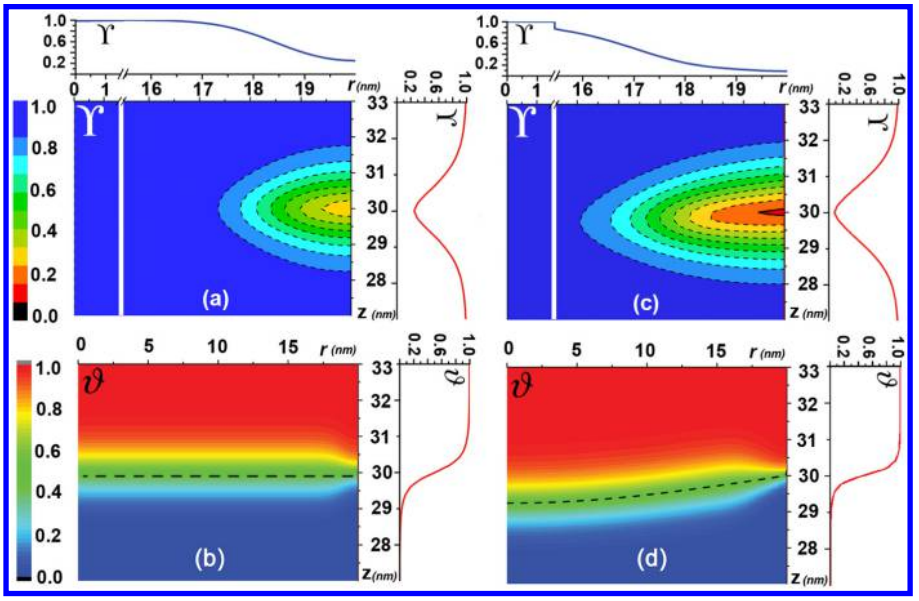

Figure 4. Structure for the CN_2 with IM at the surface of the sample. Simulations are performed at θ_e = 432*K*, k_δ = 0.7, and k_E = 2.6 for the case without (a,b) and with mechanics (c,d). Profile of order parameter $\Upsilon(r)$ along the horizontal line z = 30 nm is plotted in the top insets. Vertical insets show the profile of $\Upsilon(z)$ (top plots) and $\vartheta(z)$ (bottom plots) at r = 20 nm.

with initial conditions close to the final configuration of the CN.

We consider a cylindrical sample of R = 20 nm in radius, 100 nm in length along the axis of symmetry (z-axis), and capped by two so-called "perfectly matched" layers of 10 nm in length at the top and bottom that are used in the COMSOL code[17] to mimic an infinite sample length. Here, we focused on the effect of internal stresses and assumed that all external surfaces are stress-free. Boundary conditions for both order parameters are imposed in the form of zero normal components of the gradient of the order parameters, which will guarantee that the outer surface energy remain fixed during a PT. Two CN were considered; in one, CN_1, the IM is at the center of a sample, and in the other, CN_2, the IM is at the surface. Initial conditions for the simulations are obtained from the analytical solution for a two-phase interface profile for ϑ and two back-to-back interface profiles for Υ (see these conditions in the Supporting Information and ref 11).

In Figure 3, for solutions that are without (do not consider) mechanics (Figure 3a,b) and those with (that do consider) mechanics (Figure 3c,d), we plot the distributions of the order parameters, Υ and ϑ, revealing the structure of CN for the case when IM is at the center of a sample. Similar results for CN_2 are presented in Figure 4. The solutions were tested to make sure that they correspond to the energy min−max of the system. This test was done by taking the calculated solutions for CN

DOI: 10.1021/nl504380c
Nano Lett. 2015, 15, 2298−2303

and slightly perturbing the CN solutions toward S_1S_2 and S_1MS_2 solutions, obtaining nominally super- and subcritical nuclei. These are then used as the initial conditions for the time-dependent Ginzburg–Landau and mechanics equations. As required for the unstable CN, the solutions with sub- and supercritical IM nuclei evolved to the two stable S_1S_2 and S_1MS_2 interfaces, respectively.

For models both without and with mechanics, the CN_1 with the IM at the center has an ellipsoidal shape with $\Upsilon_{min} = 0.24$ and 0.30, respectively. The larger Υ_{min} value for the sample with mechanics is due to additional driving force associated with the relaxation of elastic energy during melting. Allowing for mechanics led to the formation of curved (bent) S_1S_2 interface, which is due to monotonically increasing volumetric transformation strain across the S_1S_2 interface. This bending cannot be realized within the usual sharp-interface approaches, suggesting that sharp-interface models should be improved to include this phenomenon, for example, in refs 18 and 19. The same interface bending is observed for CN_2 (Figure 4). Both CN change local interface structure in terms of narrowing S_1S_2 interface in ϑ distribution within CN.

By construction, the energy of both bulk solid phases is equal at their equilibrium temperature (with and without mechanics) and thus the excess interface energy is calculated with respect to any of homogeneous solid phase by integration of total energy distribution over the sample. In such a way, we determine the energy E_{ss} of the S_1S_2 and the energy E_{sms} of the S_1MS_2 ground states. Similarly, we define the energy E_1^{CN} of the CN_1 and the energy E_2^{CN} of the CN_2. The difference between the energy of each CN_1 and CN_2, and each ground state gives the activation energies for the corresponding PTs. Thus, the activation energy of the S_1MS_2 CN_1 at the center within S_1S_2 interface is $Q_{sms}^1 = E_1^{CN} - E_{ss}$ and for CN_2 at the surface is $Q_{sms}^2 = E_2^{CN} - E_{ss}$. Similar, the activation energy of the S_1S_2 CN_1 within S_1MS_2 interface is $Q_{ss}^2 = E_1^{CN} - E_{sms}$ and for CN_2 is $Q_{sm}^2 = E_2^{CN} - E_{sms}$. Each of the above-mentioned energies, which we will designate by Ψ for conciseness, is the sum of three contributions: thermal energy Ψ^θ, gradient energy Ψ^∇, and elastic energy Ψ^e. Our calculations for the energies of ground states and critical nuclei are listed in Table 1.

Table 1. Total Energy, $\Psi = \Psi^\theta + \Psi^\nabla + \Psi^e$, and Its Individual Contributing Terms, Thermal Ψ^θ Plus Gradient Ψ^∇ Energies, and Elastic Ψ^e Energy, Calculated for Ground States, E_{ss} and E_{sms}, as Well as for Interfaces with CN, E_1^{CN} with the IM at the Center of a Sample and E_2^{CN} with the IM at the Surface[a]

	without mechanics	with mechanics		
	Ψ	$\Psi^\theta + \Psi^\nabla$	Ψ^e	Ψ
E_{ss}	1256.64	1269.281	21.4274	1290.7084
E_1^{CN}	1262.684	1269.444	21.6346	1291.0786
Q_{sms}^1	6.05	0.163	0.2072	0.37
E_{sms}	1162.2663	1172.7927	12.7266	1185.5193
E_2^{CN}	1323.0063	1277.2457	17.9696	1295.2153
Q_{ss}^2	160.74	104.453	5.243	109.7
Q_{sms}^2	66.3663	7.965	−3.4578	4.507
Q_{ss}^1	100.418	96.6513	8.908	105.56

[a]Activation energies Q for appearance of the CN are the difference between energies of interfaces with CN and ground states. Simulations are performed for the cases without and with mechanics at $\theta_e = 432$ K for $k_\delta = 0.7$ and $k_E = 2.6$. All the energies are expressed in ($\times 10^{-18}J$).

A thermally activated process can be experimentally observed if the activation energy of CN is smaller than $(40-80)k_B\theta$ (ref 20), where k_B is the Boltzmann constant. This is equal to $0.24-0.48 \times 10^{-18}J$ at $\theta_e = 432$ K. The results indicate that the only possible thermally activated process is the formation of CN_1 of IM within the S_1S_2 interface at the center of a sample when mechanics is included. Because the activation energy for resolidification is much larger than the magnitude of thermal fluctuations for both CN, the IM persists. Perhaps the most surprising result is that including the energy of elastic stresses reduced the activation energy for IM critical nucleus at the center of a sample, by a factor of 16, making nucleation possible despite large undercoolings. Similarly, internal stresses significantly reduced energy of IM critical nucleus at the surface (by $\sim 62 \times 10^{-18}J$ or by a factor of 15) and the energy of the SS critical nucleus with solid at the center (by $\sim 51 \times 10^{-18}J$). Although elastic energy makes a positive contribution to the energy of ground states and CN, it increases the energy of ground states more than it increases the energy of CN. The proximate cause of this phenomenon is the slight change in the structure of the CN and alteration of the interface geometry during appearance of the CN. Thus, a small change in two large numbers (E_1^{CN} and E_{ss}) significantly changes their small difference Q_{sms}^1. To ensure that our conclusions are physical rather than due to numerical errors, we used different integration volumes enclosing IM critical nucleus. The calculations are insensitive to the integration volume as long as boundaries of this volume are far (>5 nm) from the boundaries of CN. We note that mechanics surprisingly increases activation energy for resolidification for CN_1.

Without and with mechanics, activation energies for both the IM critical nucleus and the CN of a solid–solid interface are much smaller (by $\sim 60 \times 10^{-18}J$) for the CN_1 at the center in comparison with the CN_2 at the surface. While results for CN_1 are independent of the sample size and boundary conditions for the order parameter (because CN_1 is much smaller than the sample), this is not the case for the CN_2 at the surface. Reducing the sample size reduces volume of the CN_2 and its activation energy, and for some critical size nucleation of the IM at the surface may be kinetically possible. Also, if surface energy of the melt is smaller than the surface energy of the solid, it promotes thermally activated nucleation of the IM at the surface and may also lead to barrierless nucleation. This can be studied using methods similar to those in refs 21–24. A tensorial transformation strain for melting[25] and the effect of an external load can be easily included as well. All these factors may lead to new results and phenomena.

Previous results[11] without mechanics showed very high activation energy and the practical impossibility of thermally activated intermediate melting, which contradicted the experimentally observed thermally activated interface kinetics and the overall kinetics for HMX.[1,2] The inclusion of elastic stresses in the model results in a drastic reduction of activation energy, resolving this discrepancy.

Concluding Remarks. We have developed a phase-field approach and applied it to study the effect of mechanics on barrierless and thermally activated nucleation and disappearance of nanoscale IM within an S_1S_2 interface during S_1S_2 PTs $120K$ below the melting temperature. For different ratios k_E and k_δ, various types of behavior, mechanics, and scale effects are obtained. Barrierless intermediate melting/resolidification can be continuous (reversible), jumplike in one direction and continuous in another, and jumplike in both directions

DOI: 10.1021/nl504380c
Nano Lett. 2015, 15, 2298–2303

(hysteretic), partial and complete, with monotonous and nonmonotonous dependence on k_δ and with IM-free gap region between two IM regions along k_δ axis. Internal elastic stresses only slightly promote barrierless IM nucleation but change type of system behavior, including appearance of IM for $k_E < 2$ (which is thermodynamically impossible without mechanics) and elimination of IM-free gap region. To study thermally activated nucleation, solutions for CN at the center and surface of a sample are found and activation energies are calculated and compared with the required values from a kinetic nucleation criterion. We revealed an unanticipated, drastic (16 times for HMX energetic crystals) reduction in the activation energy of IM critical nucleus when elastic energy is taken into account. This reduction results in the system meeting the kinetic nucleation criterion for the CN_1 at the center of a sample, consistent with experiments for HMX. Because thermally activated resolidification is kinetically impossible, IM persists during S_1MS_2 interface propagation. For smaller sample diameters and/or reduction of surface energy during melting, mechanics can induce IM nucleation at the surface as well. Similar effects are expected to occur for other material systems where solid−solid phase transformations via IM takes place, including electronic (Si and Ge), geological (ice, quartz, and coesite), pharmaceutical (avandia), ferroelectric ($PbTiO_3$), colloidal, and superhard (BN) materials. Similar approach can be developed for grain-boundary melting[26] and formation of interfacial and intergranular crystalline or amorphous phases (complexions)[27−30] in ceramic and metallic systems and developing corresponding interfacial phase diagrams.

■ ASSOCIATED CONTENT

Supporting Information

Details of the mathematical model and material properties. This material is available free of charge via the Internet at http://pubs.acs.org.

■ AUTHOR INFORMATION

Corresponding Author

*E-mail: vlevitas@iastate.edu.

Notes

The authors declare no competing financial interest.

■ ACKNOWLEDGMENTS

This work was supported by ONR, NSF, ARO, DARPA, and NIST. Certain commercial software and materials are identified in this report in order to specify the procedures adequately. Such identification is not intended to imply recommendation or endorsement by the National Institute of Standards and Technology, nor is it intended to imply that the materials or software identified are necessarily the best available for the purpose.

■ REFERENCES

(1) Levitas, V. I.; Henson, B. F.; Smilowitz, L. B.; Asay, B. W. *Phys. Rev. Lett.* **2004**, *92*, 235702.
(2) Levitas, V. I.; Henson, B. F.; Smilowitz, L. B.; Asay, B. W. *J. Phys. Chem. B* **2006**, *110*, 10105−10119.
(3) Henson, B. F.; Smilowitz, L.; Asay, B. W.; Dickson, P. M. *J. Chem. Phys.* **2002**, *117*, 3780−3788.
(4) Smilowitz, L.; Henson, B. F.; Asay, B. W.; Dickson, P. M. *J. Chem. Phys.* **2002**, *117*, 3789−3798.
(5) Levitas, V. I. *Phys. Rev. Lett.* **2005**, *95*, 075701.
(6) Randzio, S. L.; Kutner, A. *J. Phys. Chem. B* **2008**, *112*, 1435−1444.
(7) Levitas, V. I.; Ren, Z.; Zeng, Y.; Zhang, Z.; Han, G. *Phys. Rev. B* **2012**, *85*, 220104.
(8) Levitas, V. I.; Ravelo, R. *Proc. Natl. Acad. Sci. U.S.A.* **2012**, *109*, 13204−13207.
(9) Ball, P. *Nat. Mater.* **2012**, *11*, 747−747.
(10) Peng, Y.; Wang, F.; Wang, Z.; Alsayed, A. M.; Zhang, Z.; Yodh, A. G.; Han, Y. *Nat. Mater.* **2015**, *14*, 101−108.
(11) Momeni, K.; Levitas, V. I. *Phys. Rev. B* **2014**, *89*, 184102.
(12) Levitas, V. I.; Momeni, K. *Acta Mater.* **2014**, *65*, 125−132.
(13) Tiaden, J.; Nestler, B.; Diepers, H. J.; Steinbach, I. *Physica D* **1998**, *115*, 73−86.
(14) Folch, R.; Plapp, M. *Phys. Rev. E* **2005**, *72*, 011602.
(15) Tóth, G. I.; Pusztai, T.; Tegze, G.; Tóth, G.; Gránásy, L. *Phys. Rev. Lett.* **2011**, *107*, 175702.
(16) Mishin, Y.; Boettinger, W. J.; Warren, J. A.; McFadden, G. B. *Acta Mater.* **2009**, *57*, 3771−3785.
(17) *COMSOL Multiphysics*, version 4.2; COMSOL, Inc.: Burlington, MA, 2011,
(18) Javili, A.; Steinmann, P. *Int. J. Solids. Struct.* **2010**, *47*, 3245−3253.
(19) Levitas, V. I. *J. Mech. Phys. Solids* **2014**, *70*, 154−189.
(20) Porter, D. *Phase Transformation in Metals and Alloys*; Van Nostrand Reinhold: New York, 1981.
(21) Levitas, V. I.; Samani, K. *Nat. Commun.* **2011**, *2*, 284−6.
(22) Levitas, V. I.; Javanbakht, M. *Phys. Rev. Lett.* **2011**, *107*, 175701.
(23) Levitas, V., Javanbakht, M. *Phys. Rev. Lett.* **2010***105*.
(24) Levitas, V. I.; Samani, K. *Phys. Rev. B* **2014**, *89*, 075427.
(25) Levitas, V. I.; Samani, K. *Phys. Rev. B* **2011**, *84*, 140103(R).
(26) Lobkovsky, A. E.; Warren, J. A. *Physica D* **2002**, *164*, 202−212.
(27) Luo, J. *CRC Crit. Rev. Solid State* **2007**, *32*, 67−109.
(28) Luo, J.; Chiang, Y.-M. *Annu. Rev. Mater. Res.* **2008**, *38*, 227−249.
(29) Baram, M.; Chatain, D.; Kaplan, W. D. *Science* **2011**, *332*, 206−209.
(30) Frolov, T.; Olmsted, D. L.; Asta, M.; Mishin, Y. *Nat. Commun.* **2013**, *4*, 1899.

DOI: 10.1021/nl504380c
Nano Lett. 2015, 15, 2298−2303